

# Correlative Atomic Coordination and Interfacial Charge Polarity in $\text{Al}_2\text{O}_3/\text{GaN}$ and $\text{Al}_2\text{O}_3/\text{Si}$ Heterostructures

Chuanju Wang and Xiaohang Li\*

$\text{Al}_2\text{O}_3$  is used to form  $\text{Al}_2\text{O}_3/\text{GaN}$  and  $\text{Al}_2\text{O}_3/\text{Si}$  heterostructures for many electronic and optoelectronic devices. Yet the origins of the positive interfacial charges in the  $\text{Al}_2\text{O}_3/\text{GaN}$  heterostructure and negative interfacial charges in the  $\text{Al}_2\text{O}_3/\text{Si}$  heterostructure are often elusive. Herein, in-depth studies of the  $\text{Al}_2\text{O}_3/\text{GaN}$  and  $\text{Al}_2\text{O}_3/\text{Si}$  heterostructures are conducted, especially on how the atomic coordination structure affects the interfacial charges. It is discovered that the octahedral  $[\text{AlO}_6]^{9-}$  coordination surpassed tetrahedral  $[\text{AlO}_4]^{5-}$  coordination at the  $\text{Al}_2\text{O}_3/\text{GaN}$  interface, whereas tetrahedral  $[\text{AlO}_4]^{5-}$  coordination dominated at the  $\text{Al}_2\text{O}_3/\text{Si}$  interface. Therefore, the interfacial charge polarity is correlated with the nonstoichiometry atomic coordination of  $\text{Al}_2\text{O}_3$  at the two interfaces. This study reveals the atomic origin of charge polarity at high- $k$ /semiconductor interfaces and could facilitate the development of high-performance optoelectronic and electronic devices through engineering the atomic coordination structure of the high- $k$  materials.

the gate breakdown voltage.<sup>[10–12]</sup> By simply extending the gate dielectric thickness, enhancement-model (E-mode) GaN HEMTs can be achieved if the charges at the  $\text{Al}_2\text{O}_3/\text{GaN}$  interface are also negative.<sup>[12]</sup> Nevertheless, positive charges that occur at the  $\text{Al}_2\text{O}_3/\text{GaN}$  interface can negatively shift the threshold voltage ( $V_{\text{TH}}$ ), retarding the achievement of E-mode GaN HEMTs.<sup>[13–15]</sup> During the atomic layer deposition (ALD) process, the incomplete oxidation of trimethylamine precursors will result in residual carbon impurities in  $\text{Al}_2\text{O}_3$ , which is proposed as the origin of the positive interfacial charges of the  $\text{Al}_2\text{O}_3/\text{GaN}$  heterostructure.<sup>[16,17]</sup> Additionally, Al interstitials and O vacancies in  $\text{Al}_2\text{O}_3$  are also regarded as the sources of the positive interfacial charges in  $\text{Al}_2\text{O}_3$ .<sup>[9,18]</sup> Moreover, the

## 1. Introduction


High- $k$  dielectrics are widely used in electronic and optoelectronic devices to passivate the dangling bonds at the semiconductor surfaces or as gate insulators to reduce the gate leakage current.<sup>[1–11]</sup> However, substantial interfacial charges that occur at high- $k$  dielectric/semiconductor interfaces can severely impact device design and engineering, and the charge origins are often elusive.<sup>[1–11]</sup> For example,  $\text{Al}_2\text{O}_3$  has been adopted in many crucial devices including GaN high-electron-mobility transistors (HEMTs) and Si solar cells. In Si solar cells,  $\text{Al}_2\text{O}_3$  is used as the surface passivation layer owing to high-density negative charges occur the  $\text{Al}_2\text{O}_3/\text{Si}$  interface.<sup>[2–6]</sup> These negative charges can shield the electrons from the Si surface thus mitigating the surface recombination rate. Structural impurities in  $\text{Al}_2\text{O}_3$  such as Al vacancies, O dangling bonds, O interstitials, and H interstitials are proposed to be the origin of the negative charges.<sup>[7–9]</sup>

$\text{Al}_2\text{O}_3$  has also been widely used in GaN HEMTs as the gate dielectric to decrease the gate leakage current and increase

polarity of GaN (Ga-polar and N-polar) has negligible influence on the positive interfacial charges occur at the  $\text{Al}_2\text{O}_3/\text{GaN}$  heterostructure.<sup>[19]</sup>

The flat-band voltage ( $V_{\text{FB}}$ ) dependence on the gate dielectric thickness of  $\text{Al}_2\text{O}_3/\text{GaN}$  and  $\text{Al}_2\text{O}_3/\text{Si}$  metal-oxide-semiconductor (MOS) capacitors is shown in Figure 1a,b, respectively, where the  $V_{\text{FB}}$  was derived from the capacitance–voltage ( $C$ – $V$ ) characteristics.<sup>[19,20]</sup> The  $V_{\text{FB}}$  decreases linearly with the increased  $\text{Al}_2\text{O}_3$  thickness of the  $\text{Al}_2\text{O}_3/\text{GaN}$  MOS capacitor, whereas, it increases linearly with the increased  $\text{Al}_2\text{O}_3$  thickness of the  $\text{Al}_2\text{O}_3/\text{Si}$  MOS capacitor, indicating positive and negative charges occur at the  $\text{Al}_2\text{O}_3/\text{GaN}$  and  $\text{Al}_2\text{O}_3/\text{Si}$  interfaces, respectively. This result also implies that the charges which can affect the  $V_{\text{FB}}$  of the devices are not intrinsic to ALD  $\text{Al}_2\text{O}_3$ ; instead, semiconductor surfaces can play an important role in determining the polarity of the interfacial charges. In addition, as shown in Figure 1a,b (dotted line), positive charges can occur at other high- $k$ /GaN interfaces, such as  $\text{NiO}/\text{GaN}$ ,  $\text{HfO}_2/\text{GaN}$ , and  $\text{CeO}_2/\text{GaN}$ .<sup>[20,21]</sup> Similarly, the negative charges also occur at the interfaces between these high- $k$  dielectrics and Si.<sup>[20,21]</sup> Nonstoichiometry atomic ratios of  $\text{Al}_2\text{O}_3$  were found in the  $\text{Al}_2\text{O}_3/\text{GaN}$  and  $\text{Al}_2\text{O}_3/\text{Si}$  heterostructures where Al and O dominate at the  $\text{Al}_2\text{O}_3/\text{GaN}$  and  $\text{Al}_2\text{O}_3/\text{Si}$  interfaces, respectively.<sup>[1–3,5,6,22]</sup> In this work, we found the atomic coordination structure of  $\text{Al}_2\text{O}_3$  was also different on the GaN and Si surfaces which could explain the different interfacial charge polarity of the  $\text{Al}_2\text{O}_3/\text{GaN}$  and  $\text{Al}_2\text{O}_3/\text{Si}$  heterostructures. Moreover, this mechanism could possibly be adopted to explain the interfacial charges that occur at other high- $k$ /semiconductor interfaces.

C. Wang, X. Li  
Advanced Semiconductor Laboratory, Electrical and Computer Engineering Programs  
CEMSE Division  
King Abdullah University of Science and Technology (KAUST)  
Thuwal 23955, Saudi Arabia  
E-mail: xiaohang.li@kaust.edu.sa

 The ORCID identification number(s) for the author(s) of this article can be found under <https://doi.org/10.1002/pssr.202200413>.

DOI: 10.1002/pssr.202200413

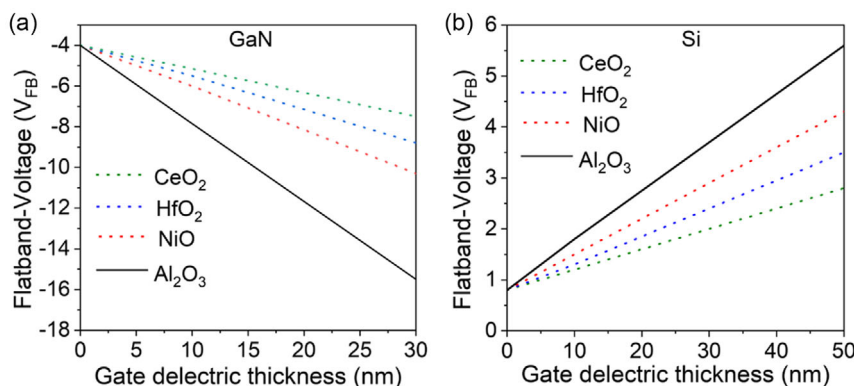


**Figure 1.** a) Calculated  $V_{FB}$  of: a) GaN and b) Si metal-oxide-semiconductor (MOS) capacitors as a function of the gate oxide thickness.<sup>[19,20]</sup>

## 2. Results and Discussion

The C–V technique was commonly used to characterize the fixed charge and trap states at the  $\text{Al}_2\text{O}_3/\text{GaN}$  and  $\text{Al}_2\text{O}_3/\text{Si}$  interfaces. The results of C–V measurements depend on the electric field distribution at the interfaces of the  $\text{Al}_2\text{O}_3/\text{GaN}$  and  $\text{Al}_2\text{O}_3/\text{Si}$  heterostructures. However, the introduction of the metal gate contact in the MOS capacitors could change the electric field distribution at the interfaces. In contrast, KPFM can provide a noninvasive and nondestructive method for mapping the surface potential of different materials.<sup>[23–25]</sup> Therefore, in this study, we used KPFM to evaluate the charge polarity and density at the interfaces of the  $\text{Al}_2\text{O}_3/\text{GaN}$  and  $\text{Al}_2\text{O}_3/\text{Si}$  heterostructures. After coating  $\text{Al}_2\text{O}_3$  onto the GaN and Si samples, the electric field induced by the charges at the interfaces of the  $\text{Al}_2\text{O}_3/\text{GaN}$  and  $\text{Al}_2\text{O}_3/\text{Si}$  heterostructures can lead to surface band bending; therefore, the changing surface potential of the bare GaN and Si samples can be probed without introducing the metal gate contact in the  $\text{Al}_2\text{O}_3/\text{GaN}$  and  $\text{Al}_2\text{O}_3/\text{Si}$  heterostructures using KPFM.

**Figure 2** illustrates that the mean potential was reduced from 993 to 661 mV after the bare, clean GaN samples were coated with a thin  $\text{Al}_2\text{O}_3$  layer; however, the mean potential increased from 305 to 737 mV after the bare, clean Si samples were coated with a thin  $\text{Al}_2\text{O}_3$  layer. In addition, after coating  $\text{Al}_2\text{O}_3$ , the root mean square roughness increased from 0.57 to 0.63 nm and from 0.48 to 0.75 nm for GaN and Si, respectively, implying the high-quality of ALD  $\text{Al}_2\text{O}_3$  layers. This indicates that GaN and Si samples have different potential responses after they are covered with a thin  $\text{Al}_2\text{O}_3$  layer (having opposite interfacial charges). This phenomenon also proves that positive charges at the  $\text{Al}_2\text{O}_3/\text{GaN}$  interface and negative charges at the  $\text{Al}_2\text{O}_3/\text{Si}$  interface were introduced after  $\text{Al}_2\text{O}_3$  deposition. The charge densities  $\sigma$  at the  $\text{Al}_2\text{O}_3/\text{GaN}$  and  $\text{Al}_2\text{O}_3/\text{Si}$  interfaces can be estimated using the Gauss theorem shown in equation<sup>[25]</sup>

$$\sigma = \frac{\Delta V_{\text{Al}_2\text{O}_3} \epsilon_{\text{Al}_2\text{O}_3} \epsilon_0}{d} \quad (1)$$

where  $\Delta V_{\text{Al}_2\text{O}_3}$  is the contact potential difference;  $\epsilon_{\text{Al}_2\text{O}_3}$  is the dielectric constant of  $\text{Al}_2\text{O}_3$ ;  $d$  is the thickness of  $\text{Al}_2\text{O}_3$ ;  $e$  is the elementary charge. Assuming that all the charges are located

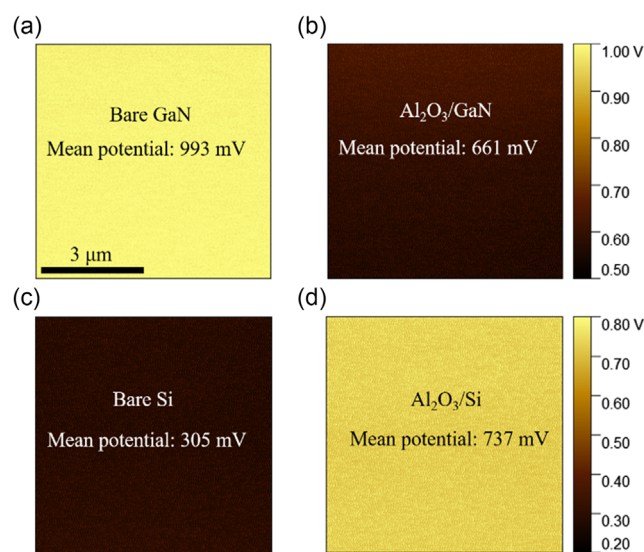


**Figure 2.** Kelvin probe force microscopy (KPFM) images of the: a) bare, clean GaN samples, b)  $\text{Al}_2\text{O}_3/\text{GaN}$ , c) bare, clean Si samples, and d)  $\text{Al}_2\text{O}_3/\text{Si}$ .

at the  $\text{Al}_2\text{O}_3/\text{GaN}$  and  $\text{Al}_2\text{O}_3/\text{Si}$  interfaces, and  $\epsilon_{\text{Al}_2\text{O}_3} = 4$  for the ultrathin  $\text{Al}_2\text{O}_3$ .<sup>[26]</sup> The charges at the  $\text{Al}_2\text{O}_3/\text{GaN}$  and  $\text{Al}_2\text{O}_3/\text{Si}$  interfaces are  $+4.5 \times 10^{12}$  and  $-5.7 \times 10^{12} \text{ cm}^{-2}$ , respectively. The interfacial charges obtained by the KPFM measurement are close to the values measured by the C–V technique.<sup>[1,11]</sup>

Electron energy loss spectroscopy (EELS) is capable of fingerprinting different coordinated forms of the same element. Amorphous  $\text{Al}_2\text{O}_3$  contains both tetrahedral  $[\text{AlO}_4]^{5-}$  and octahedral  $[\text{AlO}_6]^{9-}$  coordination; therefore, the tetrahedrally and octahedrally coordinated Al with the energy loss of 2.4 eV in separate can be mapped across the interfacial regions of the  $\text{Al}_2\text{O}_3/\text{GaN}$  and  $\text{Al}_2\text{O}_3/\text{Si}$  heterostructures by EELS measurements.<sup>[27–31]</sup> EELS has been applied to characterize the  $\text{Al}_2\text{O}_3/\text{Si}$  heterostructure, and the tetrahedral  $[\text{AlO}_4]^{5-}$  coordination was found to dominate at the interface.<sup>[27–29,32]</sup> This study employs the identical method to measure the Al coordination at the  $\text{Al}_2\text{O}_3/\text{GaN}$  interface. **Figure 3a,b** shows the STEM images of the  $\text{Al}_2\text{O}_3/\text{GaN}$  and  $\text{Al}_2\text{O}_3/\text{Si}$  heterostructures, respectively,

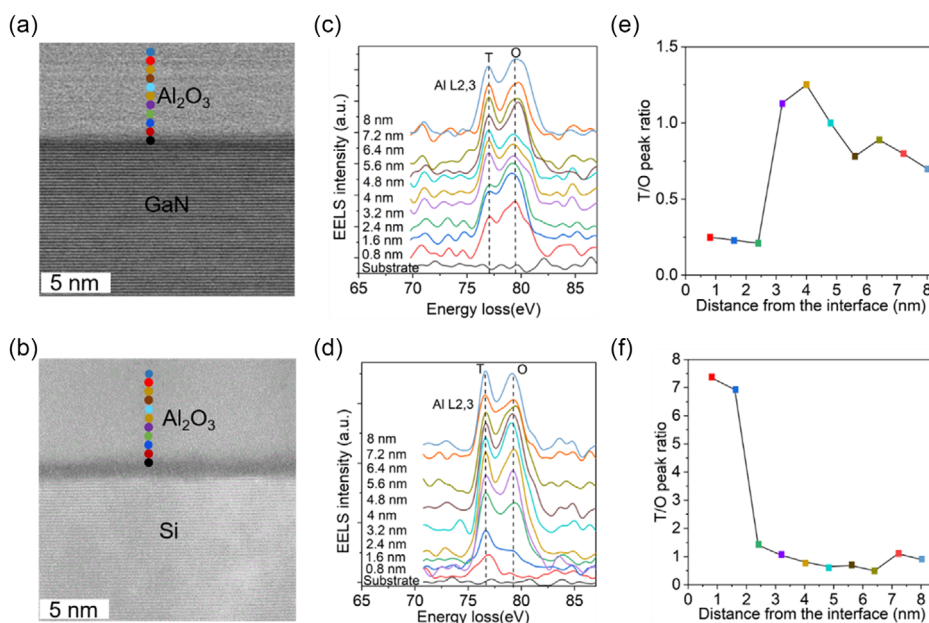


**Figure 3.** Cross-sectional scanning transmission electron microscope (STEM) images of the: a) Al<sub>2</sub>O<sub>3</sub>/GaN and b) Al<sub>2</sub>O<sub>3</sub>/Si heterostructures. The spatially resolved electron energy loss spectroscopy (EELS) spectra of Al L<sub>2,3</sub> edge across the interfacial regions from the: c) GaN and d) Si substrates to the Al<sub>2</sub>O<sub>3</sub>. Ratios of the tetrahedral (T) and octahedral (O) peak intensity as a function of the distance from the interfaces of the: e) Al<sub>2</sub>O<sub>3</sub>/GaN and f) Al<sub>2</sub>O<sub>3</sub>/Si heterostructures to the Al<sub>2</sub>O<sub>3</sub>.

and the surface oxides of GaN and Si were observed at interfaces. Figure 3c,d shows the spatially resolved EELS spectra of Al L<sub>2,3</sub> edge across the interfacial regions from the GaN and Si substrates to the Al<sub>2</sub>O<sub>3</sub> (the interval of each spectrum is 0.8 nm in distance). The black spectrum that represents the EELS from the native oxides of GaN and Si shows a negligible Al L<sub>2,3</sub> signal. For the Al<sub>2</sub>O<sub>3</sub>/GaN heterostructure, when the acquisition position is 0.8 nm away from the interface, the octahedrally coordinated Al peaks at 79.3 eV are clearly evident in the spectrum while the tetrahedrally coordinated Al peaks at 76.9 eV have small intensity. When the sampling position distance is 3.2 nm away from the interface, there occurs a dramatic increase of the tetrahedrally coordinated Al. The EELS spectra across the interfacial region from the Si substrate to the Al<sub>2</sub>O<sub>3</sub> layer was also measured. For the Al<sub>2</sub>O<sub>3</sub>/Si heterostructure, tetrahedrally coordinated Al peaks at 76.9 eV is clearly evident in the spectrum when the acquisition position is at a distance of 0.8 nm from the interface; the octahedrally coordinated Al located at 79.3 eV increases abruptly when the sampling position is at a distance of 2.4 nm from the interface. As shown in Figure 3e,f, a quantitative analysis reveals that the octahedral [AlO<sub>6</sub>]<sup>9-</sup> coordination dominates at the Al<sub>2</sub>O<sub>3</sub>/GaN interface whereas tetrahedral [AlO<sub>4</sub>]<sup>5-</sup> coordination dominates at the Al<sub>2</sub>O<sub>3</sub>/Si interface, and the tetrahedral/octahedral (T/O) peak ratio gradually increases and decreases to  $\approx 0.7$  for the Al<sub>2</sub>O<sub>3</sub>/GaN and Al<sub>2</sub>O<sub>3</sub>/Si heterostructures, respectively. Therefore, the stoichiometric derivation of the atomic coordination from the bulk Al<sub>2</sub>O<sub>3</sub> is confirmed at both the Al<sub>2</sub>O<sub>3</sub>/GaN and Al<sub>2</sub>O<sub>3</sub>/Si interfaces using the EELS measurements.

At the Al<sub>2</sub>O<sub>3</sub>/Si interface, stoichiometry deviation of O/Al ratios was widely reported where O significantly suppress Al.<sup>[1–3,5,6,22]</sup> In addition, at the surface of the Si substrate, Si

in the SiO<sub>x</sub> films has a tetrahedral coordination.<sup>[5]</sup> The physical connection of tetrahedrally coordinated Si and Al<sub>2</sub>O<sub>3</sub> leads to the dominant formation of the tetrahedrally coordinated Al at the Al<sub>2</sub>O<sub>3</sub>/Si interface.<sup>[22,33]</sup> For III-nitride materials such as AlN and GaN, octahedrally coordinated O–III–O is formed at the surfaces.<sup>[34]</sup> Similarly, octahedrally coordinated O–III–O can also imprint their structures onto the adjacent interfacial Al<sub>2</sub>O<sub>3</sub>, leading to the dominance of octahedrally coordinated Al at the Al<sub>2</sub>O<sub>3</sub>/GaN interface. Moreover, as the tetrahedral [AlO<sub>4</sub>]<sup>5-</sup> coordination peaks at 76.9 eV are O-rich,<sup>[22]</sup> nonstoichiometry O/Al ratios found in previous reports can be attributed to the dominant formation of tetrahedral [AlO<sub>4</sub>]<sup>5-</sup> coordination at the Al<sub>2</sub>O<sub>3</sub>/Si interface. At the Al<sub>2</sub>O<sub>3</sub>/GaN interface, nonstoichiometry atomic ratios of Al<sub>2</sub>O<sub>3</sub> were also found where Al significantly suppress O,<sup>[1]</sup> which can be attributed to the dominance of octahedral [AlO<sub>6</sub>]<sup>9-</sup> coordination at the interface. To explore how different atomic coordinations can affect the interfacial charge polarity, DFT calculations were performed on the heterostructures where excess Al and O were introduced at the Al<sub>2</sub>O<sub>3</sub>/GaN and Al<sub>2</sub>O<sub>3</sub>/Si interfaces, respectively.

Bader charge analysis was performed to quantitatively analyze the electron accumulation and depletion of each atom in the Al<sub>2</sub>O<sub>3</sub>/GaN heterostructures without and with the excess Al interstitial and the Al<sub>2</sub>O<sub>3</sub>/Si heterostructures without and with the excess O interstitial. Figure 4a,b shows the quantitative results of the charge change of each atom of the Al<sub>2</sub>O<sub>3</sub>/GaN heterostructures without and with one Al interstitial, respectively. Figure 4c,d shows the quantitative results of the charge change of each atom of the Al<sub>2</sub>O<sub>3</sub>/Si heterostructures without and with one O interstitial, respectively. The Al interstitial of the Al<sub>2</sub>O<sub>3</sub>/GaN heterostructure and the O interstitial of the Al<sub>2</sub>O<sub>3</sub>/Si heterostructure are indicated by arrows in Figure 4b,



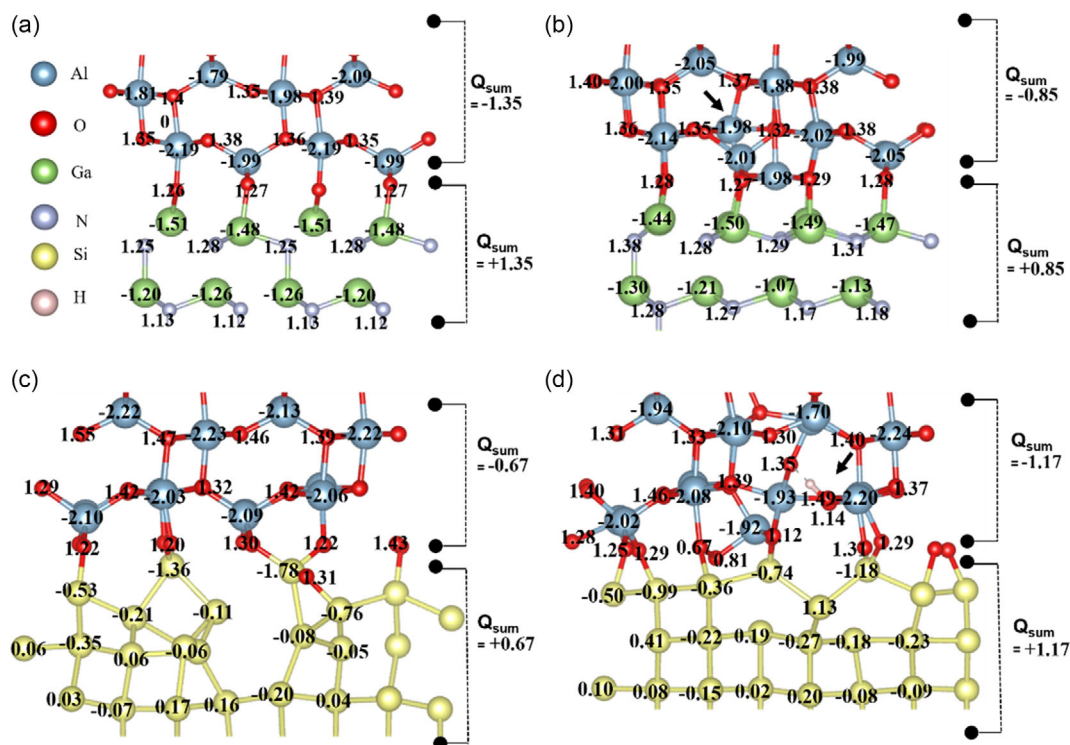


**Figure 4.** Atomic Bader charges of the  $\text{Al}_2\text{O}_3/\text{GaN}$  heterostructures: a) without and b) with one Al interstitial. Atomic Bader charges of the  $\text{Al}_2\text{O}_3/\text{Si}$  heterostructures: c) without and d) with one O interstitial. The gain and loss of electron density on each atom are indicated by the (+) and (–) signs, respectively.

d, respectively. Similar to the Al and O atoms in the lattice sites, the Al and O interstitials have an electron loss of 1.98 e and an electron gain of 1.49 e, respectively. The sum of Bader atomic charges ( $Q_{\text{sum}}$ ) is also shown in Figure 4a–d. The electron gain of  $\text{Al}_2\text{O}_3$  in the  $\text{Al}_2\text{O}_3/\text{GaN}$  heterostructures will be reduced from 1.35 to 0.85 e when the Al interstitial exists at the interface, indicating the Al interstitial will deplete electrons and induce positive interfacial charges. On the contrary, at the interface of the  $\text{Al}_2\text{O}_3/\text{Si}$  heterostructures, the electron gain increases from 0.67 to 1.17 e after interposing the O interstitial, indicating the O interstitial will accumulate electrons and induce negative interfacial charges. Therefore, atomic-coordination-induced nonstoichiometry atomic ratios at the  $\text{Al}_2\text{O}_3/\text{GaN}$  and  $\text{Al}_2\text{O}_3/\text{Si}$  interfaces are correlated to the interfacial charge polarity by DFT calculations. Indeed, Lucovsky postulated that  $\text{Al}_2\text{O}_3$  comprises both negatively charged tetrahedrally and positively charged octahedrally coordinated units and different atomic coordination should maintain a ratio to ensure charge neutrality.<sup>[5,35]</sup> Therefore, the positive interfacial charges of the  $\text{Al}_2\text{O}_3/\text{GaN}$  heterostructure and the negative interfacial charges at the  $\text{Al}_2\text{O}_3/\text{Si}$  heterostructure can be attributed to the dominance of octahedrally and tetrahedrally units at the  $\text{Al}_2\text{O}_3/\text{GaN}$  and  $\text{Al}_2\text{O}_3/\text{Si}$  interfaces, respectively.

### 3. Conclusion

In summary, different interfacial charge polarities occurring at the  $\text{Al}_2\text{O}_3/\text{GaN}$  and  $\text{Al}_2\text{O}_3/\text{Si}$  heterostructures were correlated

with the atomic coordination and nonstoichiometry atomic ratios of the interfacial  $\text{Al}_2\text{O}_3$ . Moreover, we suppose this phenomenon can also be applied to explain the charges that occur at the interfaces of  $\text{NiO}/\text{GaN}$ ,  $\text{HfO}_2/\text{GaN}$ ,  $\text{CeO}_2/\text{GaN}$ ,  $\text{NiO}/\text{Si}$ ,  $\text{HfO}_2/\text{Si}$ , and  $\text{CeO}_2/\text{Si}$ , which need further study.

### 4. Experimental Section

The n-type Si (100) and the Ga-polar GaN (0001) grown on c-plane sapphire substrates were successively cleaned with acetone, isopropanol, and deionized water. After the solvent cleaning process, the samples were immediately transferred to an ALD chamber for the  $\text{Al}_2\text{O}_3$  deposition at 300 °C. The growth per cycle was  $1.2 \text{ Å s}^{-1}$  measured by ellipsometry. For the Kelvin probe force microscopy (KPFM) measurements, 2 nm  $\text{Al}_2\text{O}_3$  was deposited onto the GaN and Si. 10 nm  $\text{Al}_2\text{O}_3$  was also deposited onto the GaN and Si samples for scanning transmission electron microscope (STEM) and electron energy loss spectroscopy (EELS) measurements. The STEM sample was fabricated by a focused ion beam (Helios G4, FEI) technique. The EELS spectroscopy was acquired using a Titan G2 60-300 (FEI) operated at 300 kV, equipped with a spherical aberration corrector. The step for each EELS acquisition is 0.8 nm, and the pixel time is 0.02 s.

Density functional theory (DFT) calculations were carried out to analyze the impact of the Al and O defects on the electronic properties of the  $\text{Al}_2\text{O}_3/\text{GaN}$  and  $\text{Al}_2\text{O}_3/\text{Si}$  heterostructures. DFT calculations were carried out with the Perdew–Burke–Ernzerhof version generalized gradient approximation for the exchange–correlation potential. The cutoff energy was set to 450 eV, and a  $6 \times 6 \times 1$  k-mesh was used. Geometry relaxations were done until the energy convergence criterion of 0.02 eV Å and the force of  $10^{-5}$  eV was achieved. The  $\theta$ -phase  $\text{Al}_2\text{O}_3$  structure was used to build the  $\text{Al}_2\text{O}_3/\text{GaN}$  and  $\text{Al}_2\text{O}_3/\text{Si}$  heterostructures, as its bandgap and mass density values were close to ALD  $\text{Al}_2\text{O}_3$ .<sup>[36]</sup> The wurtzite GaN and cubic Si

phases were adopted in the heterojunctions. Structural optimization was first applied to the separated GaN and Si structures. Next, the Al<sub>2</sub>O<sub>3</sub>/GaN and Al<sub>2</sub>O<sub>3</sub>/Si heterostructures were built up without and with defects. Pseudohydrogen atoms were adopted to passivate the N dangling bonds at the bottom of the Al<sub>2</sub>O<sub>3</sub>/GaN heterostructure and Si dangling bonds at the bottom Al<sub>2</sub>O<sub>3</sub>/Si heterostructure thus guaranteeing that all the density of states originated from the defects at the interfaces. For the Al<sub>2</sub>O<sub>3</sub>/GaN heterostructure, pseudohydrogen atoms with 0.75 valence electrons were used. For the Al<sub>2</sub>O<sub>3</sub>/Si heterostructures, pseudohydrogen atoms with one valence electron were used.<sup>[37]</sup> Then, the structural optimization was repeated.

## Acknowledgements

The authors would like to acknowledge the support of KAUST Baseline BAS/1/1664-01-01, Near-term Grand Challenge Fund REI/1/4999-01-01, Competitive Research Grant URF/1/4374-01-01, and Impact Acceleration Fund REI/1/5124-01-01.

## Conflict of Interest

The authors declare no conflict of interest.

## Data Availability Statement

The data that support the findings of this study are available from the corresponding author upon reasonable request.

## Keywords

atomic coordination, interfaces, negative charges, positive charges

Received: October 28, 2022

Revised: December 3, 2022

Published online: December 28, 2022

- [1] C. Wang, F. AlQatari, V. Khandelwal, R. Lin, X. Li, *Appl. Surf. Sci.* **2022**, 608, 155099.
- [2] F. Werner, B. Veith, D. Zielke, L. Kühnemund, C. Tegenkamp, M. Seibt, R. Brendel, A. P. Schmidt, **2011**, 109, 113701.
- [3] V. Naumann, M. Otto, R. B. Wehrspohn, S. Hagendorf, *J. Vac. Sci. Technol. A: Vac. Surf. Films*, **2012**, 30, 04D106.
- [4] V. Naumann, M. Otto, R. Wehrspohn, M. Werner, C. Hagendorf, *Energy Proc.* **2012**, 27, 312.
- [5] B. Hoex, J. Gielis, M. Van de Sanden, W. Kessels, *J. Appl. Phys.* **2008**, 104, 113703.
- [6] B. Hoex, J. Schmidt, R. Bock, P. Altermatt, M. Van De Sanden, W. Kessels, *Appl. Phys. Lett.* **2007**, 91, 112107.
- [7] D. Hiller, P. M. Jordan, K. Ding, M. Pomaska, T. Mikolajick, D. König, *J. Appl. Phys.* **2019**, 125, 015301.
- [8] D. Hiller, D. Tröger, M. Grube, D. König, T. Mikolajick, *J. Phys. D: Appl. Phys.* **2021**, 54, 275304.
- [9] M. Choi, A. Janotti, C. G. Van de Walle, *J. Appl. Phys.* **2013**, 113, 044501.
- [10] K. Kim, J. H. Ryu, J. Kim, S. J. Cho, D. Liu, J. Park, I.-K. Lee, B. Moody, W. Zhou, J. Albrecht, *ACS Appl. Mater. Interfaces* **2017**, 9, 17576.
- [11] A. Hiraiwa, K. Horikawa, H. Kwarada, *J. Appl. Phys.* **2021**, 129, 195303.
- [12] L. Vauche, A. Chanuel, E. Martinez, M.-C. Roure, C. Le Royer, S. Bécu, R. Gwoziecki, M. Plissonnier, *Materials* **2021**, 3, 1170.
- [13] K. Aoshima, M. Horita, J. Suda, T. Hashizume, *Appl. Phys. Express* **2021**, 14, 015501.
- [14] Y. Ando, M. Deki, H. Watanabe, N. Taoka, A. Tanaka, S. Nitta, Y. Honda, H. Yamada, M. Shimizu, T. Nakamura, *Appl. Phys. Express* **2021**, 14, 081001.
- [15] Y. Ando, K. Nagamatsu, M. Deki, N. Taoka, A. Tanaka, S. Nitta, Y. Honda, T. Nakamura, H. Amano, *Appl. Phys. Lett.* **2020**, 117, 102102.
- [16] M. Choi, J. L. Lyons, A. Janotti, C. G. Van de Walle, *Appl. Phys. Lett.* **2013**, 102, 142902.
- [17] X. Liu, C. Jackson, F. Wu, B. Mazumder, R. Yeluri, J. Kim, S. Keller, A. Arehart, S. Ringel, J. Speck, *J. Appl. Phys.* **2016**, 119, 015303.
- [18] J. Weber, A. Janotti, C. Van de Walle, *J. Appl. Phys.* **2011**, 109, 033715.
- [19] T.-H. Hung, S. Krishnamoorthy, M. Esposto, D. Neelim Nath, P. Sung Park, S. Rajan, *Appl. Phys. Lett.* **2013**, 102, 072105.
- [20] F. Roccaforte, P. Fiorenza, G. Greco, R. L. Nigro, F. Giannazzo, A. Patti, M. Saggio, *Phys. Status Solidi A* **2014**, 211, 2063.
- [21] R. Lo Nigro, P. Fiorenza, G. Greco, E. Schilirò, F. Roccaforte, *Materials* **2022**, 15, 830.
- [22] D. K. Simon, P. M. Jordan, T. Mikolajick, I. Dirnstorfer, *ACS Appl. Mater. Interfaces* **2015**, 7, 28215.
- [23] V. Aubriet, K. Courouble, M. Gros-Jean, Ł. Borowik, *Rev. Sci. Instrum.* **2021**, 92, 083905.
- [24] P. A. F. Garrillo, Ł. Borowik, F. Caffy, R. Demadrille, B. Grévin, *ACS Appl. Mater. Interfaces* **2016**, 8, 31460.
- [25] W. Song, J. Chen, Z. Li, X. Fang, *Adv. Mater.* **2021**, 2101059.
- [26] A. Henning, J. D. Bartl, A. Zeidler, S. Qian, O. Bienek, C. M. Jiang, C. Paulus, B. Rieger, M. Stutzmann, I. D. Sharp, *Adv. Funct. Mater.* **2021**, 31, 2101441.
- [27] G. Noircler, F. Lebreton, E. Drahi, P. de Coux, B. Warot-Fonrose, *Micron* **2021**, 145, 103032.
- [28] K. Kimoto, Y. Matsui, T. Nabatame, T. Yasuda, T. Mizoguchi, I. Tanaka, A. Toriumi, *Appl. Phys. Lett.* **2003**, 83, 4306.
- [29] A. Konashuk, A. Sokolov, V. Drozd, F. Schaefer, E. Filatova, *Thin Solid Films* **2013**, 534, 363.
- [30] D. Bouchet, C. Colliex, *Ultramicroscopy* **2003**, 96, 139.
- [31] E. Schilirò, P. Fiorenza, C. Bongiorno, C. Spinella, S. Di Franco, G. Greco, R. Lo Nigro, F. Roccaforte, *AIP Adv.* **2020**, 10, 125017.
- [32] B. Hoex, M. Bosman, N. Nandakumar, W. Kessels, *Phys. Status Solidi* **2013**, 7, 937.
- [33] D. Hiller, *ACS Appl. Mater. Interfaces* **2018**, 10, 30495.
- [34] Z. Fang, E. Wang, Y. Chen, X. Hou, K.-C. Chou, W. Yang, J. Chen, M. Shang, *ACS Appl. Mater. Interfaces* **2018**, 10, 30811.
- [35] G. Lucovsky, *J. Vac. Sci. Technol.* **1981**, 19, 456.
- [36] Z. Zhang, Y. Guo, J. Robertson, *Appl. Phys. Lett.* **2019**, 114, 161601.
- [37] J. Li, L.-W. Wang, *Phys. Rev. B* **2005**, 72, 125325.